Instantons in chiral magnets

Masaru Hongo, Toshiaki Fujimori, Tatsuhiro Misumi, Muneto Nitta, and Norisuke Sakai

Phys. Rev. B **101**, 104417 — Published 23 March 2020

DOI: 10.1103/PhysRevB.101.104417

Instantons in Chiral Magnets

Masaru Hongo,[1,2,3,*] Toshiaki Fujimori,[1,†]
Tatsuhiro Misumi,[4,1,2,‡] Muneto Nitta,[1,§] and Norisuke Sakai[1,2,¶]

[1] *Department of Physics, and Research and Education Center for Natural Sciences, Keio University, 4-1-1 Hiyoshi, Yokohama, Kanagawa 223-8521, Japan*
[2] *iTHEMS, RIKEN, Wako, Saitama 351-0198, Japan*
[3] *Department of Physics, University of Illinois, Chicago, IL 60607, USA*
[4] *Department of Mathematical Science, Akita University, 1-1 Tegata-Gakuen-machi, Akita 010-8502, Japan*

We exhaustively construct instanton solutions and elucidate their properties in one-dimensional anti-ferromagnetic chiral magnets based on the $O(3)$ nonlinear sigma model description of spin chains with the Dzyaloshinskii-Moriya (DM) interaction. By introducing an easy-axis potential and a staggered magnetic field, we obtain a phase diagram consisting of ground-state phases with two points (or one point) in the easy-axis dominant cases, a helical modulation at a fixed latitude of the sphere, and a tri-critical point allowing helical modulations at an arbitrary latitude. We find that instantons (or skyrmions in two-dimensional Euclidean space) appear as composite solitons in different fashions in these phases: temporal domain walls or wall-antiwall pairs (bions) in the easy-axis dominant cases, dislocations (or phase slips called meron) with fractional instanton numbers in the helical state, and isolated instantons and calorons living on the top of the helical modulation at the tri-critical point. We also show that the models with DM interaction and an easy-plane potential can be mapped into those without them, providing a useful tool to investigate the model with the DM interaction.

I. INTRODUCTION

Topological excitations (topological solitons and instantons) play key roles in various systems from particle physics[1–3] and cosmology[4] to condensed matter systems[5,6]. Amongst various examples, magnets allow magnetic skyrmions and domain walls in spin systems[7–10], and in particular, chiral magnets with the Dzyaloshinskii-Moriya (DM) interaction[11,12] is a representative where topological excitations play a pivotal role for applications to nano-devices such as magnetic memories. Recent theoretical and experimental developments have confirmed that there exists the so-called chiral soliton lattice phase — aligning helical domain walls —in one-dimensional ferromagnetic spin chains[13–15]. More recently, a skyrmion lattice in two-dimensional (2D) chiral ferromagnets and associated peculiar transport phenomena have been experimentally observed[16–19] (See e. g.[20–23] for related theoretical works). Furthermore, magnetic monopoles have been recently paid much attention. They appear for unwinding a skyrmion line in a skyrmion lattice[24] and form a stable crystal in certain parameter region[25]. Anti-ferromagnetic chiral magnets have been also studied both in experimental and theoretical sides[26–30].

One of recent interesting theoretical developments might be the finding of a critical coupling at which the strength of DM interaction and Zeeman magnetic field or magnetic anisotropy are balanced[31–34], analogous to superconductors at the critical coupling between types I and II. In this case, it allows so-called Bogomol'yi-Prasad-Sommerfield (BPS) topological solitons[35,36], *i. e.* the most stable configurations with a fixed boundary condition (or a topological sector), which were originally found for magnetic monopoles and other topological solitons in high energy physics and now are realized in superconductors at the critical coupling.

Despite of such experimental and theoretical developments, instantons[37,38] (see Refs.[1–3]) – classical solutions of Euclidian field theory and one of the most crucial theoretical concepts to understand physical properties of quantum systems –have never been studied thus far in chiral magnets. They represent nonperturbative quantum effects coming from nontrivial saddle point solutions of the Euclidian path integral. With the help of instantons, we can understand several key results of physical systems such as a ground-state property of non-abelian gauge theory[39–43] and nonlinear sigma models.

In this paper, we work out instantons in chiral magnets. After presenting a phase diagram, we exhaustively provide instanton solutions in one-dimensional anti-ferromagnetic spin chains with the DM interaction: temporal domain walls, domain wall-antidomain wall pair (called bions), vortices or dislocations as fractional instantons (called merons), and BPS instantons and calorons at the critical coupling, corresponding to the so-called Kaplan-Shekhtman-Aharony-Entin-Wohlman (KSAE) limit[44,45]. The constructed instanton solutions can also describe various skyrmion configurations in two (spatial) dimensional chiral ferromagnets and anti-ferromagnets with an anisotropic DM interaction in one direction.

The organization of the paper is as follows: In Sec. II, we introduce the model and clarify the classical ground state phase diagram. In Sec. III, we construct various instanton solutions away from the tri-critical point. In Sec. IV, we discuss a simple BPS instanton and periodic instanton (caloron) solutions at the tri-critical point. In Sec. V, we show an equivalence theorem between the

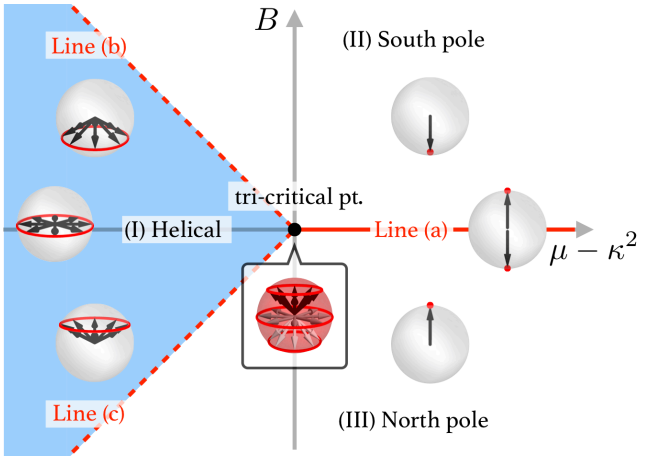

Fig. 1. Phase diagram of the $O(3)$ nonlinear sigma model with the DM interaction at the classical level.

	OPM G/H	π_0	π_1	π_2	π_3
(I)	S^1	0	$\mathbb{Z}$	0	0
(a)	$\mathbb{Z}_2$	$\mathbb{Z}_2$	0	0	0
Tri-critical pt.	$O(3)/O(2) \simeq S^2$	0	0	$\mathbb{Z}$	$\mathbb{Z}$
(II) (III) (b)(c)	1pt	0	0	0	0

TABLE I. The OPMs and associated homotopy groups.

models with and without the DM interaction within our model. Sec. VI is devoted to the summary and discussion. In Appendices A and B, we present a derivation of our field-theoretical model from a lattice spin model, and the spatial-domain wall solution, respectively.

II. MODEL AND GROUND STATE

Magnetic spin texture in quantum spin-chain is described in the continuum limit by a unit Néel vector n^a $(a = 1, 2, 3)$ with $\sum_a n^a n^a = 1$. The energy functional for one-dimensional spin-chain involving the DM interaction with the strength κ in addition to the kinetic term, easy-axis potential and staggered magnetic field is given at low-energy as a form of the $O(3)$ or $\mathbb{C}P^1$ sigma model:

$$E[n] = \int \mathrm{d}x \left[\frac{(\partial_x n^a)^2}{2} + \kappa(n^1 \partial_x n^2 - n^2 \partial_x n^1) + \mu \frac{1 - (n^3)^2}{2} + B n^3 \right]. \quad (1)$$

For $\mu > 0$, the potential favors for n^a to point to the north $(n^3 = 1)$ or the south $(n^3 = -1)$ pole (easy-axis). For $\mu < 0$, it favors the equator $(n^3 = 0)$ (easy-plane). In sharp contrast to the real magnetic field, which resutls in the quadratic potential term in the effective Lagrangian (See e. g. Ref.[46]), the term Bn^3 linearly coupled to the Néel vector n^a is a staggered magnetic field, but, for simplicity, we will call B as a magnetic field.

Since the DM interaction can be regarded as a background gauge field[34], the energy can be rewritten by defining a covariant derivative $D_x n^a \equiv \partial_x n^a - \kappa \epsilon^{3ab} n^b$ as

$$E[n] = \int \mathrm{d}x \left[\frac{(D_x n^a)^2}{2} + (\mu - \kappa^2) \frac{1 - (n^3)^2}{2} + B n^3 \right]. \quad (2)$$

Since the first nonnegative term must vanish for a ground state, we obtain[47]

$$D_x n^a = 0 \quad (a = 1, 2, 3), \quad (3)$$

which has the helical-state solution given by

$$n^1 + \mathrm{i} n^2 = A \mathrm{e}^{-\mathrm{i}\kappa x}, \; n^3 = \pm\sqrt{1 - |A|^2} \quad (4)$$

with $A \in \mathbb{C}$ satisfying $|A| \leq 1$. This is the spatially modulated state, where n^a rotates at a constant latitude of the S^2 target space with the wave number κ along the spatial direction x. The actual minimum of $E[n]$ depends on the value of the easy-axis potential μ and the magnetic field B. By examining the minimum of the potential as a function of n^3, we find three critical lines emanating from the tri-critical point at $\mu = \kappa^2$, $B = 0$ as illustrated in Fig. 1: the line (a) along $B = 0$, $\mu > \kappa^2$, the line (b) along $\kappa^2 - \mu = B > 0$, and the line (c) along $\kappa^2 - \mu = -B > 0$. The ground state of the chiral magnet is helical states in the region (I) the south pole in the region (II) and the north pole in the region (III), respectively (See Fig. 1). At the tri-critical point $B = 0$, $\mu = \kappa^2$, all the helical states with $|A| \leq 1$ become the ground states with the same energy. It is interesting to observe that the DM interaction tends to favor easy-plane configuration, so that helical ground states can be ground states even in the presence of the easy-axis potential with $\mu > 0$. In experiment, typical values of order $\kappa \approx 0.03(\text{Å})^{-1}$, $\mu \approx (0.01)(\text{Å})^{-2}$ with vanishing B are realized in (2d) material such as $Ba_2CuGe_2O_7$[27,30]. Note that these values corresponding to almost tri-critical point ones.

The order of phase transition for the critical lines are as follows: The first-order phase transition occurs on the line (a), since the global minimum of the energy jumps from one local minimum to the other across (a). The second-order phase transition occurs on the lines (b) and (c), where the second derivative of the ground state energy density with respect to B is discontinuous. It is also notable that the tri-critical point, which is a switching point of the first- and second-order transitions, has a larger symmetry as we will discuss in detail later.

The topology of the order parameter manifold (OPM) G/H is summarized in Table I: S^2 at the tri-critical point, two discrete points (the north and south poles) along the line (a), S^1 in the region (I), a point (north pole) in the region (II) including the line (b), and a point (south pole) in the region (III) including the line (c). The homotopy class $\pi_n(G/H)$ of OPM determines allowed types of instanton solutions. For instance, $\pi_1(S^1) = \mathbb{Z}$ in the region (I) and $\pi_0(\mathbb{Z}_2) = \mathbb{Z}_2$ on the line (a) supports vortex and domain wall solutions, both hosting instantons

In order to explore instanton solutions for the anti-ferromagnetic material[48], we introduce the imaginary time τ and consider the following Euclidean 2D Lagrangian ($i = 0, 1$) (See Appeneix A for a derivation from a lattice spin system):

$$\begin{aligned}\mathcal{L} =& \frac{1}{2}(\partial_i n^a)^2 + \kappa(n^1\partial_x n^2 - n^2\partial_x n^1) \\ &+ \frac{\mu}{2}[1-(n^3)^2] + Bn^3.\end{aligned} \tag{5}$$

Note that this Euclidean 2D model should also be useful to describe the energy density of a 2+1D magnetic material (both ferromagnetic and anti-ferromagnetic) which has an anisotropic uniaxial DM interaction only in one spatial direction x rather than two spatial directions. It is also convenient to use the stereographic projection of the target space $n^a \in S^2$ to a complex plane $v \in \mathbb{C}$ through

$$v = \frac{n^1 + \mathrm{i}n^2}{1+n^3}, \quad n^3 = \frac{1-|v|^2}{1+|v|^2}. \tag{6}$$

The $O(3)$ sigma model with the DM interaction becomes

$$\mathcal{L} = \frac{2\{|\partial_i v|^2 + \mathrm{i}\kappa v \overset{\leftrightarrow}{\partial}_x \bar{v} + \mu|v|^2\}}{(1+|v|^2)^2} + B\frac{1-|v|^2}{1+|v|^2} \tag{7}$$

with $v\overset{\leftrightarrow}{\partial}_x\bar{v} = v\partial_x\bar{v} - \bar{v}\partial_x v$. The instanton number density ρ_Q is defined by

$$\rho_Q = \frac{1}{4\pi}\epsilon_{abc}n^a\partial_x n^b\partial_\tau n^c = \frac{1}{\pi}\frac{\partial_z v\partial_{\bar{z}}\bar{v} - \partial_{\bar{z}}v\partial_z\bar{v}}{(1+|v|^2)^2}, \tag{8}$$

where we used the complex coordinates $z = x + \mathrm{i}\tau$, $\bar{z} = x - \mathrm{i}\tau$. The integration of this quantity in the Euclidean 2D space yields the instanton number characterizing the second homotopy group π_2. Below, we show that instanton solutions exist in all the phases, sometimes as composite objects even when the OPM does not have a nontrivial π_2.

III. VARIOUS INSTANTON SOLUTIONS

In this section, based on the effective Lagrangian (5) and identified the classical phase diagram given in Fig. 1, we work out possible instanton solutions; a temporal domain wall, bion, and meron. The discussion on the BPS instanton at the tri-critical point will be given in the next section.

A. Temporal domain wall on the line (a)

In this case the OPM consists of two points, suggesting that there exists a domain wall solution connecting these two discrete ground states. Let us construct a domain wall solution in the temporal direction, regarded as an instanton, for the boundary condition $n_3(\tau = \pm\infty, x) = \pm 1$. For that purpose, we make a Bogomol'nyi completion[35,36] of the action as

$$\begin{aligned}\int \mathrm{d}^2x\,\mathcal{L} = \int \mathrm{d}x\Bigg[&\frac{2|(\partial_x + \mathrm{i}\kappa)v|^2 + 2|(\partial_\tau + \sqrt{\mu-\kappa^2})v|^2}{(1+|v|^2)^2} \\ &- \partial_\tau\frac{\sqrt{\mu-\kappa^2}}{1+|v|^2}\Bigg].\end{aligned} \tag{9}$$

Since terms in the first line are positive semi-definite, the surface term provides the lower bound of the energy:

$$\int \mathrm{d}^2x\,\mathcal{L} \geq -2\sqrt{\mu-\kappa^2}\int \mathrm{d}x\left[\frac{1}{1+|v|^2}\right]_{\tau=-\infty}^{\tau=\infty}. \tag{10}$$

The equality holds when the BPS equations

$$(\partial_x + \mathrm{i}\kappa)v = 0, \quad \partial_\tau v + \sqrt{\mu-\kappa^2}\,v = 0 \tag{11}$$

are satisfied. This equation gives the following domain wall solution with a complex integration constant C

$$v = C\mathrm{e}^{-\mathrm{i}\kappa x - \sqrt{\mu-\kappa^2}\tau}, \quad C \in \mathbb{C}, \tag{12}$$

which has unit instanton number and action $-2\sqrt{\mu-\kappa^2}$ per length $\Delta x = 2\pi/\kappa$. This is the lowest energy configuration satisfying the boundary condition. It is interesting to note that as shown in Fig. 2 (a), helical states show up only in the vicinity of the wall even though it is hidden in the ground states ($n^3 = \pm 1$). Note that we can also construct a spatial domain wall solutions with $Q = 0$ (See Appendix B).

B. Bions in the phases (II) and (III)

If the magnetic field is turned on ($B \neq 0$) in the region (II) or (III), we find that the linear term in n^3 allows non-BPS wall-antiwall solutions, so-called bion solutions[49,50]. To construct the bion solution, let us first put the ansatz

$$v = f(\tau)\mathrm{e}^{-\mathrm{i}\kappa x}, \tag{13}$$

with a real function $f(\tau)$, and derive a functional form of $f(\tau)$. Substituting this ansatz, we rewrite the equation of motion as

$$f''(\tau) - \frac{2f}{1+f^2}f'(\tau)^2 + (\kappa^2-\mu)\frac{1-f^2}{1+f^2}f + Bf = 0. \tag{14}$$

Since the system enjoys invariance under the Euclidean time shift $\tau \to \tau + a$, the Euclidean energy

$$\mathcal{E} = 2\frac{f'(\tau)^2 + (\kappa^2-\mu)f^2}{(1+f^2)^2} - B\frac{1-f^2}{1+f^2}, \tag{15}$$

gives a conserved quantity, and hence it is independent of the Euclidean time τ. From this conservation law, we

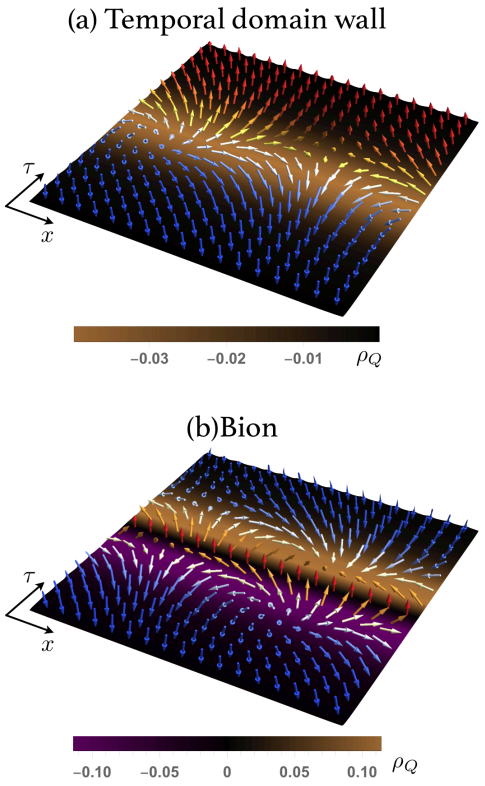

Fig. 2. (a) A temporal domain wall configuration of $\boldsymbol{n}$ interpolating two degenerate ground states, as an instanton solution. (b) Domain wall-antidomain wall pair (bion).

can obtain implicit forms of the solutions of the equation of motion as

$$\int \mathrm{d}f \left[\frac{(1+f^2)^2}{2}\left(\mathcal{E} - B\frac{1-f^2}{1+f^2}\right) - (\kappa^2-\mu)f^2\right]^{-\frac{1}{2}} = \tau. \tag{16}$$

Let us then consider configurations which approach the minimum of the potential in the limit $\tau \to \pm\infty$. At the minimum of the potential, the value of the conserved quantity is $\mathcal{E} = \pm B$ for $B > 0$ (region (II)) and $B < 0$ (region (III)), respectively. Substituting these values into Eq. (16), we find a solution

$$f(\tau) = \left(\frac{\sqrt{|B|}}{\omega}\sinh\omega\tau\right)^{\mathrm{sign}(B)}, \tag{17}$$

where we introduced $\omega = \sqrt{\mu - \kappa^2 + |B|}$. The general single bion solution can be obtained by introducing position moduli parameters τ_0 and x_0 with the help of the translational symmetry, which results in

$$v = \mathrm{e}^{-\mathrm{i}\kappa(x-x_0)}\left[\frac{\sqrt{|B|}}{\omega}\sinh\omega(\tau-\tau_0)\right]^{\mathrm{sign}(B)}. \tag{18}$$

These solutions play a vital role in nonperturbative effects and resurgence theory[49–56] recently being extensively considered in field theory[57].

C. Merons in helical state (I)

In this case, the OPM is S^1 at latitude $\sqrt{(\kappa^2-\mu+B)/(\kappa^2-\mu-B)}$. Therefore, we expect to find a vortex characterized by a non-trivial winding number around S^1. It carries a fractional instanton number[58] as is known for skyrmions with easy-plane potential[21,59,60], and is sometimes called a meron. A single-winding configuration takes the form

$$v = \mathrm{e}^{-\mathrm{i}\kappa x}\frac{z}{|z|}h(|z|), \tag{19}$$

where $z = x + \mathrm{i}\tau, \bar{z} = x - \mathrm{i}\tau$ are the complex coordinates, and $h(|z|)$ is a profile function satisfying the field equation

$$\begin{aligned} 0 = {} & h''(|z|) + \frac{1}{|z|}h'(|z|) - \frac{2h(|z|)}{1+h(|z|)^2}h'(|z|)^2 \\ & + \left[B + \frac{1-h(|z|)^2}{1+h(|z|)^2}\left(\kappa^2 - \mu - \frac{k^2}{r^2}\right)\right]h(|z|), \end{aligned} \tag{20}$$

and the boundary conditions $h(0) = 0$ and $h(\infty) = \sqrt{(\kappa^2-\mu+B)/(\kappa^2-\mu-B)}$. Numerically solving the field equation we find a meron solution in Fig. 3. Fig. 3 (a) and (b) show the configuration of a meron, which also exhibits a dislocation of the phase (or a phase slip) as shown in Fig. 3 (c).

IV. INSTANTONS AT THE TRI-CRITICAL POINT

In this section, after showing the general BPS instantion solution at the tricritical point, we describe its detailed properties living on a plane $\mathbb{R}^2$ (zero-temperature), and a cylinder $\mathbb{R}\times S^1$ (finite-temperature/ring-shaped sample).

A. BPS bound and general solution

The richest array of instantons is obtained at the tricritical point $\mu = \kappa^2$, $B = 0$, where the Euclidean 2D action is bounded by the instanton number $Q = \int d^2x\,\rho_Q$ as

$$\int \mathrm{d}^2x\,\mathcal{L}_{\mathrm{cr}} \geq \pm(4\pi Q + \int \mathrm{d}^2x\,\kappa\partial_\tau n^3). \tag{21}$$

The bound is saturated if and only if the BPS equation

$$\partial_\tau n_a \mp \epsilon_{abc}n^b D_x n^c = 0 \quad \text{or} \quad \partial_{\bar{z}}v = -\mathrm{i}\kappa v/2 \tag{22}$$

is satisfied. Let us consider solutions with a nonnegative instanton number Q (by taking the upper sign of the bound). Hence all the BPS solutions are obtained as

$$v(x,\tau) = \mathrm{e}^{-\mathrm{i}\kappa x}w(z), \tag{23}$$

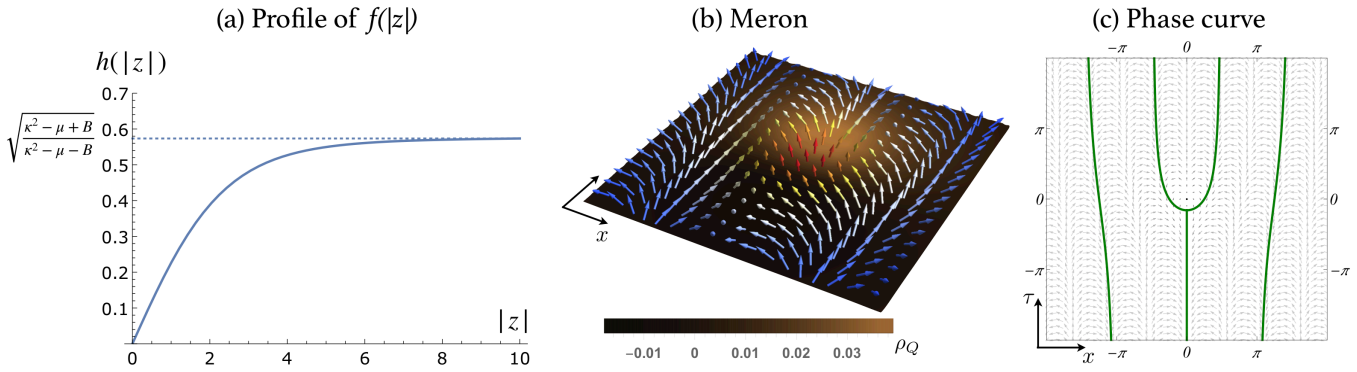

Fig. 3. (a) Profile of $h(|z|)$. (b) Meron ($\mu = 3,\ \kappa = 2,\ B = -1/2$). (c) Meron as a dislocation or phase slip. Solid lines indicate the contours with $\arg v = -\pi/2$ (or $\mathrm{Im}\,(e^{-i\kappa x} z/|z|) = -1$) and arrows denote (n_1, n_2).

with an arbitrary holomorphic function $w(z)$.

The BPS equation has the general l-instanton/caloron BPS solutions given by a rational function of degree l

$$v_{\rm inst} = \mathrm{e}^{-\mathrm{i}\kappa x}\frac{p(z)}{q(z)}, \quad v_{\rm cal} = \mathrm{e}^{-\mathrm{i}\kappa x}\frac{p(\mathrm{e}^{\mathrm{i}\frac{2\pi z}{L}})}{q(\mathrm{e}^{\mathrm{i}\frac{2\pi z}{L}})} \tag{24}$$

where $p(z)$, $q(z)$ are mutually coprime polynomials of degree m, n with $l = \max(m, n)$.

A typical configuration of the single ($l = 1$) BPS instanton is shown in Fig. 4(a). The caloron solutions are periodic instantons in the periodicity interval $x \sim x + L$. A single ($l = 1$) BPS caloron[61–63] for the case of $\kappa L/(2\pi) \in \mathbb{Z}$ is shown in Fig. 4(b).

B. The most general one instanton solution ($Q = 1$) on the plane $\mathbb{R}^2$

The most general BPS solution with the unit instanton charge $Q = 1$ is given by a rational function of degree $l = 1$: $p(z)$, $q(z)$ as polynomials of at most degree unity without a common root. We can choose the following parametrization as a convenient standard form for the most general solution which has three complex moduli parameters $z_1, z_2, \alpha \in \mathbb{C}$, with $z_1 \neq z_2$

$$v_{\rm 1inst} = \mathrm{e}^{-\mathrm{i}\kappa x}\alpha\frac{z - z_1}{z - z_2}. \tag{25}$$

The Néel vector points to the north pole $n^3 = +1$ at the zero $z = z_1$ of $v(z, \bar{z})$, and to the south pole $n^3 = -1$ at the pole $z = z_2$ of $v(z, \bar{z})$.

One can define the contour of the Néel vector rotating in the equatorial plane $n^3 = 0$ around either $z = z_1$ or $z = z_2$ as the size of the instanton, since the energy density is approximately localized in the region enclosed by the contour. We find that the size and phase moduli around $z = z_1$ are given by $(z_1 - z_2)/\alpha$ if $\alpha \gg 1$, and that the size and phase moduli around $z = z_2$ are given by $\alpha(z_2 - z_1)$ if $\alpha \ll 1$. In that sense, we can call α as a dimensionless moduli parameter to determine the size and the phase (the rotation angle in n^1, n^2 plane) of the instanton, whereas the length parameter of the instanton is given by $|z_1 - z_2|$. We note that the DM interaction parameter κ provides the period $2\pi/\kappa$ of the helical structure, which is visible in regions away from the north ($n^3 = +1$) and south ($n^3 = -1$) poles of the

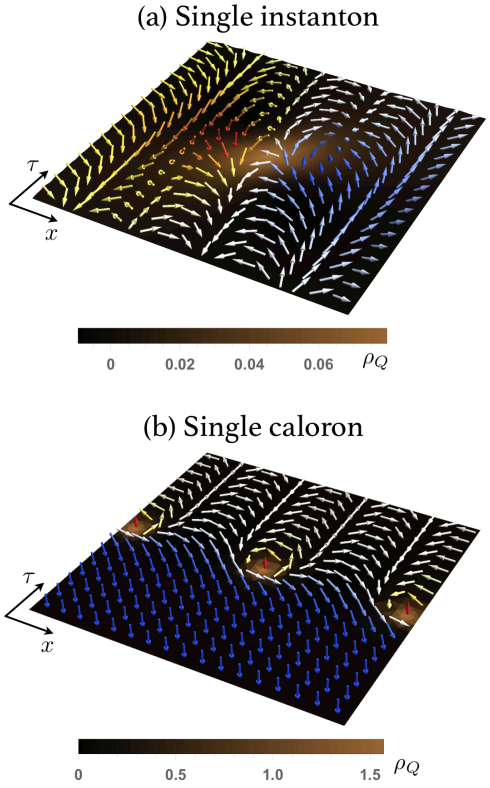

Fig. 4. Configurations of $\boldsymbol{n}$ for (a) single BPS instanton solution: $p(z)/q(z) = (z - z_0)/(z + z_0)$, and (b) single BPS caloron solution ($\kappa L = 2\pi$): $p(\mathrm{e}^{\mathrm{i}\frac{2\pi z}{L}})/q(\mathrm{e}^{\mathrm{i}\frac{2\pi z}{L}}) = \mathrm{e}^{\mathrm{i}\frac{2\pi(z-z_0)}{L}} - 1$ within two periods ($-L \leq x < L$).

Néel vector.

Fig. 5 shows the configuration of n^a of the $Q = 1$ solution (25) with a different parameter set controlling the size modulus. One should note that the spacetime volume of the figures in Fig. 5 is chosen to be $-2\pi/\kappa \leq x, \tau < 2\pi/\kappa$. Therefore the visible region of the helical modulation is the largest in the case of (iii) $|z_1 - z_2|/\alpha = 3^2$, and the smallest in the case of (i) $|z_1 - z_2|/\alpha = 1$.

In contrast, we have depicted the other extreme situation of $Q = 1$ BPS instanton solution with $\alpha = 1$ in Fig. 4 (a), where both the north pole $n^3 = +1$ at $z = z_0$ and the south pole $n^3 = -1$ at $z = -z_0$ are equally visible, and the energy density is spread equally around both of these points. This solution satisfies the boundary condition $n^3 = 0$ at infinity $z = \infty$. This also illustrates the fact that different boundary conditions generically select BPS solutions with different values of moduli parameters.

For BPS solutions with higher values of the instanton charge $Q = l$, we find $2l+1$ complex moduli parameters as coefficients of polynomials $p(z)$ and $q(z)$. They constitute generalizations of positions of the north pole ($n^3 = +1$) and the south pole ($n^3 = -1$) and the size and phase moduli of a $Q = 1$ BPS instanton solution.

C. Instanton and caloron solutions on a cylinder $\mathbb{R} \times S^1$

Another interesting family of instanton solution is obtained when we consider the system living on the compactified base space (x, τ) along one direction, or a cylinder $\mathbb{R} \times S^1$. One can think of this compactification as putting the system in a finite temperature situation for the (imaginary) time-direction, or making a ring-shaped sample of the spin chain for the spatial direction. In this setup, one need to impose a boundary condition along the compactified direction. While the most popular choice is the periodic boundary condition, there is another theoretically interesting one; the twisted boundary condition, which allows a system to have a fractional (half) instatnton number. Here we will demonstrate the half instanton solution and caloron (periodic instanton) solutions associated with the compactification.

Half instanton and caloron with time-compactification: Let us demonstrate BPS instanton solutions with the compacification along the τ direction. We here impose a general boundary condition with any twisting angle $0 \leq \delta < 2\pi$ as

$$v(x, \tau + T) = \mathrm{e}^{\mathrm{i}\delta} v(x, \tau), \tag{26}$$

which can be translated into the boundary condition on the holomorphic function $w(z)$ with the same twisting angle $w(z + \mathrm{i}T) = \mathrm{e}^{\mathrm{i}\delta} w(z)$. One can regard the twisted boundary condition (26) as introducing the imaginary chemical potential. Note that the case with $\delta = 0$ corresponds to a usual periodic (thermal) boundary condition, and $\delta = \pi$ to an anti-periodic boundary condition, which will be discussed below.

Let us first consider the anti-periodic boundary condition with $\delta = \pi$, which allows us to have a half instanton solution[61–63]. For this boundary condition, the holomorphic function $w(z)$ needs to satisfy $w(z + \mathrm{i}T) = -w(z)$, and one can easily obtain simple solutions such as $w = \mathrm{e}^{\pm\pi(z-z_0)/T}$. Thus, we find a BPS solution for the antiperiodic boundary condition

$$v(x, \tau) = \mathrm{e}^{-\mathrm{i}\kappa x} \mathrm{e}^{\pm\frac{\pi}{T}(z-z_0)}, \tag{27}$$

where a single complex moduli $z_0 \in \mathbb{C}$ has a physical meaning of the position and phase of the BPS solution. One should note that the holomorphy dictates that the boundary condition along the τ direction implies the exponential behavior along the x direction. Depending on the sign in the exponent, upper (lower) sign corresponds to the solution satisfying the boundary condition $n^3 = +1(-1)$ at $x = -\infty$ and $n^3 = -1(+1)$ at $x = -\infty$ at spatial infinity. Thus the solution is a spatial domain wall, but a difference with the usual domain wall is that phase winds half along the domain wall world line in the τ direction. It is interesting to note that the compactification together with the boundary condition along τ direction automatically dictates possible boundary conditions at spatial infinity.

Since the solution winds along the τ direction only by half rotation because of antiperiodic boundary condition, it has the half unit of instanton charge Q (with the sign). Namely, the Néel vector n^a covers only half of the sphere S^2 in this solution. The more general BPS solution with the antiperiodic boundary condition contains solutions with half odd integer Q. Fig. 6 shows the configuration of n^a of the half-instanton BPS solution in Eq. (27).

If we introduce a deformation potential proportional to the Bn^3 term, we can obtain an exact non-BPS bion solution composed of these half instanton $Q = 1/2$ and half anti-instanton $Q = -1/2$. The solution is of a similar form as the bion solution in (18), and has been found to play a vital role to understand the resurgence in the $\mathbb{C}P^1$ quantum mechanics and quantum field theory in two dimensions[49–57].

Furthermore, we can also construct a caloron solution with the twisted boundary condition (26). For instance, we can obtain a single Caloron solution centered at z_0 with the size moduli a and twisting angle δ as

$$v = \frac{T}{2\pi a} \mathrm{e}^{-\mathrm{i}\kappa x} \left(\mathrm{e}^{\frac{2\pi}{T}(z-z_0)} - 1 \right) \mathrm{e}^{\frac{(z-z_0)\delta}{T}}. \tag{28}$$

When we impose the anti-periodic boundary condition by choosing $\delta = \pi$, the caloron sotution (28) shows an interesting dependence on the compactification size T. Fig. 8 shows configurations of n^a with different size of the compactified direction[61–63]. We see that one-insanton-like configuration in the large T case changes their shape to split into the periodic configuration by taking smaller values of the compactified size.

Caloron solution with spatial compactification: If we choose the x direction to be compactified in contrast

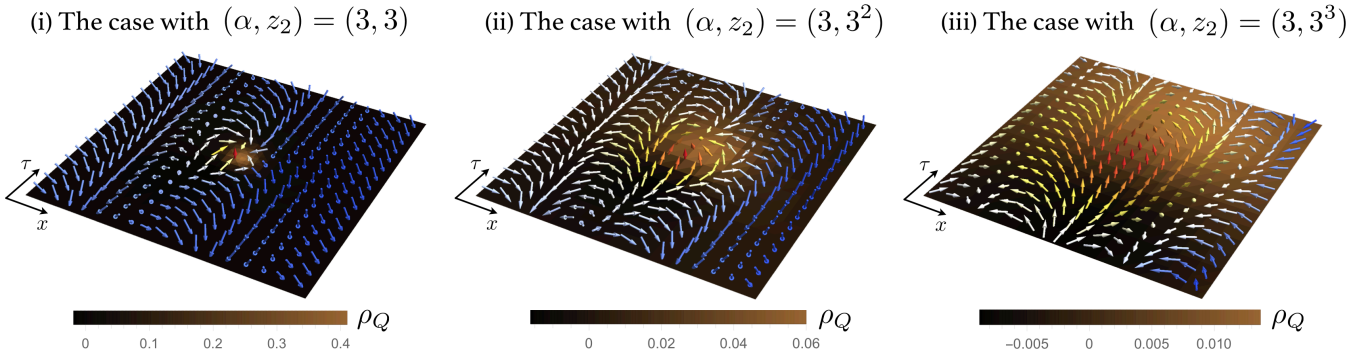

Fig. 5. Simple BPS one instanton solution (25) with different parameters with a fixed spacetime volume and $z_1 = 0$.

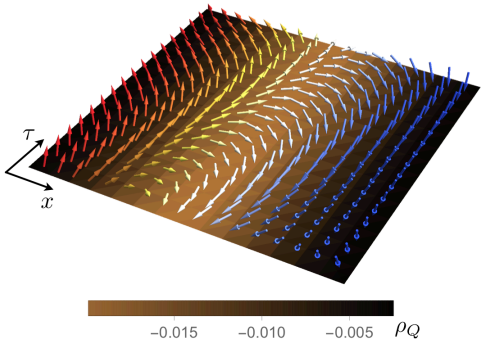

Fig. 6. Half instanton solution (27) with the antiperiodic boundary condition (26) with $\delta = \pi$.

to the τ direction, we encounter a complication when the compactification period L is not an integer multiple of $2\pi/\kappa$ (the intrinsic period of the helical state). We see that the mismatch between the DM interaction period $2\pi/\kappa$ and the compactification size L results in the induced twisting angle for the holomorphic function $w(z)$. To focus on this point, let us consider the periodic boundary condition for $v(x + L, \tau) = v(x, \tau)$, which implies that the physical Néel vector n^a is periodic. Since the BPS solution is given by $v = \mathrm{e}^{-\mathrm{i}\kappa x} w(z)$, the holomorphic function $w(z)$ has to satisfy a twisted boundary condition $w(z + L) = \mathrm{e}^{\mathrm{i}\kappa L} w(z)$. We then obtain generic BPS caloron solutions as

$$v(x,\tau) = \mathrm{e}^{-\mathrm{i}\kappa x} \mathrm{e}^{\mathrm{i}\frac{\kappa L}{2\pi}\frac{2\pi z}{L}} \frac{p(\mathrm{e}^{\frac{2\pi \mathrm{i} z}{L}})}{q(\mathrm{e}^{\frac{2\pi \mathrm{i} z}{L}})}. \tag{29}$$

Depending on the boundary condition at a spatial infinity, we have two types of solutions similarly to the half-instanton solutions in Eq. (27). For instance, defining $[X]$ as the largest integer less or equal to X, we obtain the simplest caloron with $l = 1$ with the position z_0 and size a moduli for the instanton as

$$v_+(x,\tau) = \frac{L}{2\pi \mathrm{i} a} \mathrm{e}^{-\mathrm{i}\kappa x} \mathrm{e}^{\mathrm{i}\left(\frac{\kappa L}{2\pi} - \left[\frac{\kappa L}{2\pi}\right]\right)\frac{2\pi z}{L}} \left(\mathrm{e}^{\frac{2\pi \mathrm{i}}{L}(z - z_0)} - 1\right), \tag{30}$$

which satisfies the boundary condition $n^3 = -1$ at $\tau \to -\infty$ and $n^3 = +1$ at $\tau \to \infty$, and also

$$v_-(x,\tau) = \frac{L}{2\pi \mathrm{i} a} \mathrm{e}^{-\mathrm{i}\kappa x} \mathrm{e}^{\mathrm{i}\left(\frac{\kappa L}{2\pi} - \left[\frac{\kappa L}{2\pi}\right] - 1\right)\frac{2\pi z}{L}} \left(\mathrm{e}^{\frac{2\pi \mathrm{i}}{L}(z - z_0)} - 1\right), \tag{31}$$

which satisfies the boundary condition $n^3 = +1$ at $\tau \to -\infty$ and $n^3 = -1$ at $\tau \to \infty$. We note that the instanton charge Q per unit periodicity is an integer for the caloron with the periodic boundary condition $v(x + L, \tau) = v(x, \tau)$, whereas (BPS bound for) the action per unit periodicity is not an integer multiple of 4π, as can be seen from Eq. (21). As will be discussed in the next section, we can define a new variable $\hat{n}^a$ whose instanton charge multiplied by 4π gives the BPS bound.

V. EQUIVALENCE THEOREM

Let us now show that there exists a one-to-one mapping between the above model (5) and the usual $O(3)$ sigma model. For that purpose, inspired by the helical ground states (4), we define new variables[64] $\hat{n}^a$ as

$$n^1 + \mathrm{i} n^2 = (\hat{n}^1 + \mathrm{i}\hat{n}^2)\mathrm{e}^{-\mathrm{i}\kappa x}, \quad n^3 = \hat{n}^3. \tag{32}$$

In terms of the new variables, the $O(3)$ sigma model with the DM interaction can be rewritten into that without the DM interaction $\mathcal{L}_{\mathrm{woDM}}(\hat{n}) = \mathcal{L}(n)$:

$$\mathcal{L}_{\mathrm{woDM}}(\hat{n}) = \frac{1}{2}(\partial_\mu \hat{n}^a)^2 + \frac{\mu - \kappa^2}{2}[1 - (\hat{n}^3)^2] + B\hat{n}^3. \tag{33}$$

Note that the strength of the easy-axis potential is reduced from the original one. It is also interesting to see that the BPS bound for the energy is identical to 4π times instanton charge $\hat{Q}$ in terms of the Néel vector $\hat{\boldsymbol{n}}$ of the $O(3)$ sigma model without the DM interaction in Eq. (21):

$$4\pi Q + \int d^2x \kappa \partial_\tau n^3 = 4\pi \hat{Q}. \tag{34}$$

From this equivalence theorem, we find that all instanton solutions in the $O(3)$ sigma model with the DM

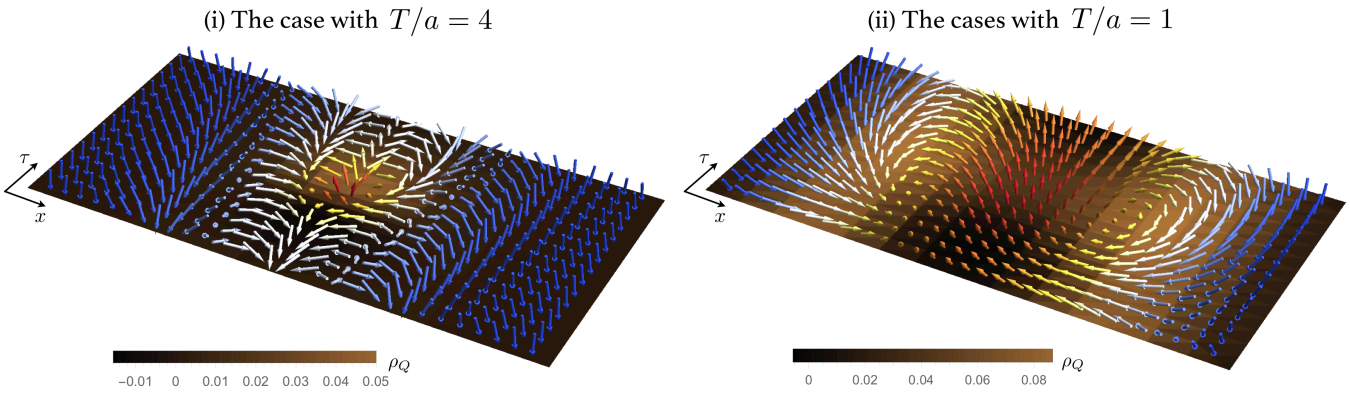

Fig. 7. Caloron solution (28) under the anti-periodic boundary condition ($\delta = \pi$).

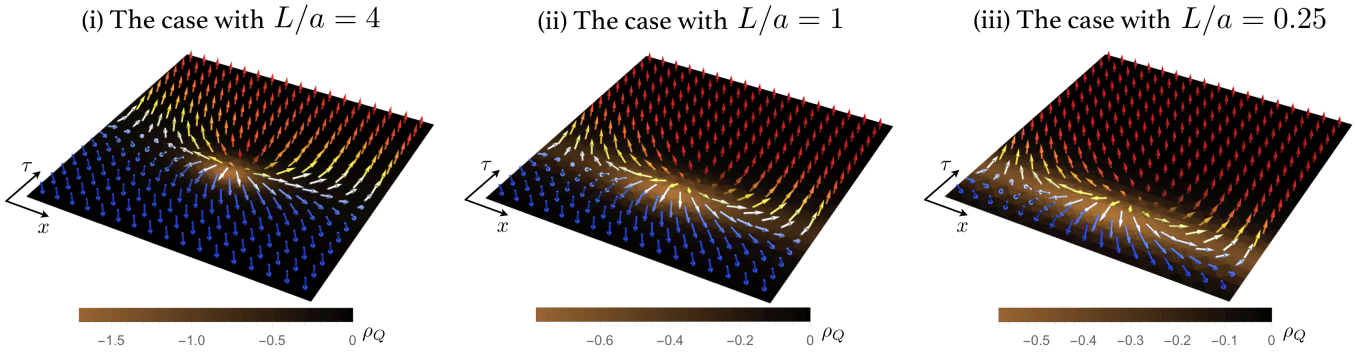

Fig. 8. Caloron solutions (31) under the periodic boundary condition along x direction.

interaction has one-to-one correspondence with those of the $O(3)$ sigma model without the DM interaction. This indicates that the original model (5) possesses a kind of hidden symmetry (known as modified symmetry[65,66]), which enables us to compactly summarize our finding on the ground states and instanton solutions (See Table I). Nevertheless, it should be emphasized that the physical variable n^a must be used to find the real magnetic texture of chiral magnets.

VI. SUMMARY AND DISCUSSION

We have clarified possible instanton solutions for the one-dimensional anti-ferromagnetic spin chain in the presence of the DM interaction. Depending on the phases, we have exhausted all possible instanton solutions including temporal domain walls with the instanton number density distributed in the temporal direction, vortices (dislocations or phase slips) as merons and BPS instantons and caloron at the critical coupling. We have also shown that the model with the DM interaction is equivalent to the model without the DM interaction.

Our results have implications both for theoretical and experimental researches. The instanton solutions in chiral magnets, which were not discussed before, give a novel theoretical insight into the anti-ferromagnetic spin chains and our methodology to obtain them based on the equivalence theorem can be applied broadly in the related studies. The phase diagram in Fig. 1 with the variety of instantons can help us to understand physics which would be observed in future experiments on chiral magnets with controllable DM interaction[67–70] or easy-axis potential.

There are several interesting avenues related to this work. While we have considered one-dimensional chiral magnets in this paper, we can generalize our approach to higher-dimensional systems[31–34]. In particular, the 2D model allows a topologically conserved skyrmion current and Hopf terms, thus involves rich theoretical structures. Although we have only focused on the ground state at the classical field level and instanton solutions interpolating them, it is also interesting to consider generic quantum aspects of the systems; e. g. a generalization of the Haldane conjecture[71,72] in chiral anti-ferromagnetic chains, and deconfined quantum criticality in $2+1$-dimensional systems[73–75]. The possible 't Hooft anomaly — field theoretical manifestation of the Lieb-Schultz-Mattis theorem[76,77] — together with semi-classics analyses including resurgence theory in the sigma models[49–56] will shed light on the detailed quantum aspects of chiral magnets.

ACKNOWLEDGMENTS

This work is supported by MEXT-Supported Program for the Strategic Research Foundation at Private Universities "Topological Science" (Grant No. S1511006) and by the Japan Society for the Promotion of Science (JSPS) Grant-in-Aid for Scientific Research (KAKENHI) Grant Number 18H01217. The authors are also supported in part by JSPS KAKENHI Grant Numbers 18K03627 (T. F.), 19K03817 (T. M.), and 16H03984 (M. N.). M.H. was also supported by the U.S. Department of Energy, Office of Science, Office of Nuclear Physics under Award Number DE-FG0201ER41195, and RIKEN iTHEMS Program (in particular, iTHEMS STAMP working group). The work of M.N. is also supported in part by a Grant-in-Aid for Scientific Research on Innovative Areas "Topological Materials Science" (KAKENHI Grant No. 15H05855) from MEXT.

Appendix A: Derivation of effective Lagrangian given in Eq. (5)

In order to discuss various instanton solutions, we rely on the continuum field-theoretical description of the antiferromagnetic spin chain, which leads to the Euclidean 2D Lagrangian for the $O(3)$ nonlinear sigma model given in Eq. (5). Starting from the lattice spin system with the DM interaction, we here give a derivation of the effective Lagrangian (See e. g. Refs.[78–80] in the absence of symmetry breaking terms).

The Hamiltonian for a 1-dimensional antiferromagnetic chiral magnet reads

$$H=\sum_i\Big[J\boldsymbol{s}_i\cdot\boldsymbol{s}_{i+1}-\boldsymbol{D}\cdot(\boldsymbol{s}_i\times\boldsymbol{s}_{i+1})+(\boldsymbol{s}_i)^tC\boldsymbol{s}_i+(-1)^i\boldsymbol{b}\cdot\boldsymbol{s}_i\Big], \tag{A1}$$

where $J(>0)$ denotes anti-ferromagnetic coupling, and $\boldsymbol{D}$ the DM interaction, C a possible anisotropic potential called the single-ion anisotropy, and $\boldsymbol{b}$ the staggered magnetic field. Considering that a possible antiferromagnetic Néel order leads to $\langle\boldsymbol{s}_i\rangle=(-1)^i s\boldsymbol{n}$, we parametrize the lattice spin variable with the lattice spacing a as[78–80]

$$\boldsymbol{s}_i=s\left[(-1)^i\boldsymbol{n}_i\sqrt{1-a^2\boldsymbol{\ell}_i^2}+a\boldsymbol{\ell}_i\right]\equiv s\boldsymbol{N}_i. \tag{A2}$$

Note that $\boldsymbol{n}_i(t)\cdot\boldsymbol{n}_i(t)=1$ and $\boldsymbol{n}_i(t)\cdot\boldsymbol{\ell}_i(t)=0$ are satisfied to respect the normalization condition $\boldsymbol{s}_i^2=s^2$ with the magnitude of the spin s. Substituting this to the Hamiltonian (A1), we perform an expansion with respect to the lattice spacing a to obtain the continuum description. The leading-order expansion results in

$$\begin{aligned}H(\boldsymbol{n})&=\sum_x\Big[\frac{Js^2a^2}{2}\big(\partial_x\boldsymbol{n}(x)\big)^2+Js^2a^2\boldsymbol{\ell}^2(x)-s^2a\boldsymbol{D}\cdot\big(\boldsymbol{n}(x)\times\partial_x\boldsymbol{n}(x)\big)+s^2\boldsymbol{n}^t(x)C\boldsymbol{n}(x)+s\boldsymbol{b}\cdot\boldsymbol{n}(x)\Big]+\cdots\\&\simeq\int\mathrm{d}x\Big[\frac{Js^2a}{2}\big(\partial_x\boldsymbol{n}(x)\big)^2+Js^2a\boldsymbol{\ell}^2(x)-s^2\boldsymbol{D}\cdot\big(\boldsymbol{n}(x)\times\partial_x\boldsymbol{n}(x)\big)+a^{-1}s^2\boldsymbol{n}^t(x)C\boldsymbol{n}(x)+a^{-1}s\boldsymbol{b}\cdot\boldsymbol{n}(x)\Big]\end{aligned} \tag{A3}$$

where, in the second line, we neglect higher-order terms (ellipsis in the first line) in powers of the lattice spacing a. Taking account of the Berry phase term $\omega[\boldsymbol{N}_i]$, the path-integral formula for the partition function $Z(\beta)\equiv\mathrm{Tr}e^{-\beta H}$ results in

$$Z(\beta)=\mathcal{N}\int\mathcal{D}\boldsymbol{n}_i\mathcal{D}\boldsymbol{\ell}_i\exp\left(-\sum_i\mathrm{i}s\omega[\boldsymbol{N}_i]-\int_0^\beta\mathrm{d}\tau H(\boldsymbol{n})\right), \tag{A4}$$

with a normalization constant $\mathcal{N}$. Substituting the above parametrization to the Berry phase term, we obtain

$$\begin{aligned}&s\sum_i\omega[\boldsymbol{N}_i]\\&=s\sum_i\left[\omega[(-1)^i\boldsymbol{n}_i]+a\int_0^\beta\mathrm{d}\tau\boldsymbol{\ell}_i(t)\cdot\left.\frac{\delta\omega[\boldsymbol{n}]}{\delta\boldsymbol{n}(t)}\right|_{\boldsymbol{n}=(-1)^i\boldsymbol{n}_i}\right]\\&=s\sum_i(-1)^i\omega[\boldsymbol{n}_i]+\int_0^\beta\mathrm{d}\tau\mathrm{d}x\boldsymbol{\ell}(x)\cdot\big(\partial_\tau\boldsymbol{n}(x)\times\boldsymbol{n}(x)\big)\end{aligned}$$

where we have used $\omega[-\boldsymbol{n}]=-\omega[\boldsymbol{n}]$ with the periodic boundary condition and the variational formula $\delta\omega[\boldsymbol{n}]/\delta\boldsymbol{n}(\tau)=\partial_\tau\boldsymbol{n}\times\boldsymbol{n}$ to obtain the second line. Assuming that the total number of sites is even, we can further simplify the first term in this equation as

$$\begin{aligned}\sum_{i=1}^{2N}(-1)^i\omega[\boldsymbol{n}_i]&=\sum_{i=1}\int_0^\beta\mathrm{d}\tau\left.\frac{\delta\omega[\boldsymbol{n}]}{\delta\boldsymbol{n}(\tau)}\right|_{\boldsymbol{n}=\boldsymbol{n}_{2i}}\cdot\delta\boldsymbol{n}_{2i}(\tau)\\&=\frac{1}{2}\int_0^\beta\mathrm{d}\tau\mathrm{d}x(\partial_\tau\boldsymbol{n}\times\boldsymbol{n})\cdot\partial_x\boldsymbol{n}=2\pi Q[\boldsymbol{n}],\end{aligned}$$

where we have defined the instanton number as

$$Q[\boldsymbol{n}]\equiv\int_0^\beta\mathrm{d}\tau\mathrm{d}x\rho_Q(\boldsymbol{n})\quad\text{with}\quad\rho_Q(\boldsymbol{n})=\frac{1}{4\pi}\epsilon_{abc}n^a\partial_xn^b\partial_\tau n^c. \tag{A5}$$

Performing the Gaussian integral for $\boldsymbol{\ell}$, we obtain the path-integral formula for the partition function as

$$Z(\beta) = \mathcal{N}' \int \mathcal{D}\boldsymbol{n} \exp\left[2\pi \mathrm{i} s Q[\boldsymbol{n}] - \int_0^\beta \mathrm{d}\tau \mathrm{d}x \left(\frac{1}{2}(\partial_i \boldsymbol{n})^2 + \boldsymbol{\kappa}\cdot(\boldsymbol{n}\times\partial_x\boldsymbol{n}) + \frac{1}{2}\boldsymbol{n}^t M \boldsymbol{n} + \boldsymbol{B}\cdot\boldsymbol{n}\right)\right]. \tag{A6}$$

with $\boldsymbol{n}^2 = 1$, and we have rescaled the space and time so that the coefficient of the kinetic term is unity. We also have renamed the coefficients (coefficient matrix M and vector $\boldsymbol{\kappa}$ and $\boldsymbol{B}$) for the symmetry breaking terms. Since the first term given by the instanton number is a total derivative, it does not affect the classical equation of motion. We also note that $Q[\boldsymbol{n}]$ takes only integer values for a sphere as the base manifold (spanned by (τ, x)), although it causes a remarkable nonperturbative quantum effect depending on the value of the spin s as was conjectured by Haldane: the integer spin case shows a gapped symmetry-protected topological phase with the so-called Haldane gap while the half-integer spin case shows a gapless conformal behavior. Let us first take $\boldsymbol{\kappa} = (0, 0, \kappa)$ as the most generic case if there are no potential terms ($M = \boldsymbol{B} = 0$). For the potential terms, we choose a special configuration for the coefficients $M = (\mu, \mu, 0)$, and $\boldsymbol{B} = (0, 0, B)$ as is often realized in experimental setups. Then we obtain

$$Z(\beta) = \mathcal{N}' \int \mathcal{D}n^a \exp\left[2\pi \mathrm{i} s Q[n^a] - \int_0^\beta \mathrm{d}\tau \mathrm{d}x \left(\frac{1}{2}(\partial_i n^a)^2 + \kappa(n^1\partial_x n^2 - n^2\partial_x n^1) + \frac{\mu}{2}\left[1-(n^3)^2\right] + Bn^3\right)\right]. \tag{A7}$$

As the action to obtain the classical equation of motion, we take only the second term, which gives the effective Lagrangian in Eq. (5) in the main text.

Appendix B: Spatial domain wall on the line (a)

In a similar manner with a domain wall instanton in the main text, we can construct a spatial domain wall solution on the line (a). We impose a boundary condition $n_3(\tau, x = \pm\infty) = \pm 1$ at the left and right spatial infinities. For a τ-independent configuration, we can make a Bogomol'nyi completion[35,36] of the energy to find

$$\int \mathrm{d}x\, \mathcal{L} = 2\int \mathrm{d}x \left[\frac{|(\partial_x + \eta)v|^2}{(1+|v|^2)^2} + \partial_x \frac{\sqrt{\mu-\kappa^2}}{1+|v|^2}\right] \tag{B1}$$

with $\eta = \sqrt{\mu-\kappa^2} + \mathrm{i}\kappa$. Since the first term is positive semi-definite, the surface term again provides the lower bound of the energy:

$$\int \mathrm{d}x\, \mathcal{L} \geq 2\sqrt{\mu-\kappa^2}\left[\frac{1}{1+|v|^2}\right]_{x=-\infty}^{x=\infty}. \tag{B2}$$

The equality holds when the BPS equation

$$(\partial_x + \mathrm{i}\kappa)v + \sqrt{\mu-\kappa^2}\, v = 0 \tag{B3}$$

is satisfied. This equation gives the following domain wall solution with a complex integration constant C

$$v = C\mathrm{e}^{-\mathrm{i}\kappa x - \sqrt{\mu-\kappa^2}x}, \quad C \in \mathbb{C}, \tag{B4}$$

which is the lowest energy configuration satisfying the boundary condition. This spatial domain wall solution exhibits the helical modulation as illustrated in Fig. 9, although it does not carry an instanton number ($Q = 0$) in contrast to the temporal domain wall solution in Eq. (12) in the main text.

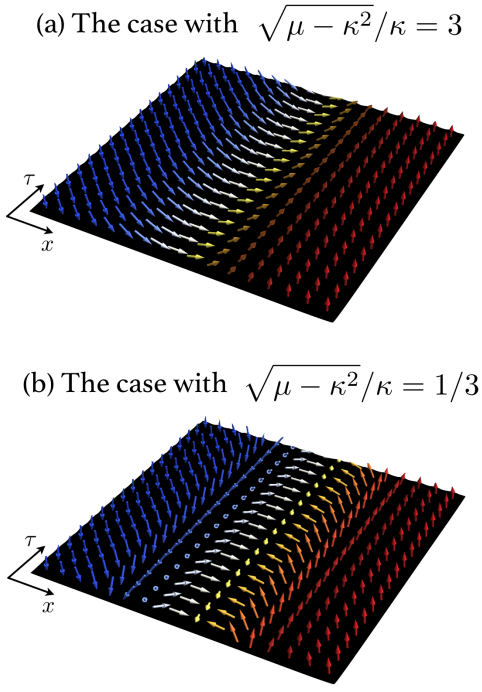

Fig. 9. Two spaitial domain wall configurations of $\boldsymbol{n}$ interpolating two degenerate ground states.

* masaru.hongo(at)riken.jp
† toshiaki.fujimori018(at)gmail.com
‡ misumi(at)phys.akita-u.ac.jp
§ nitta(at)phys-h.keio.ac.jp
¶ norisuke.sakai(at)gmail.com

[1] R. Rajaraman, *Solitons and instantons. An introduction to solitons and instantons in quantum field theory* (Amsterdam, Netherlands: North-holland (1982) 409p, 1982).
[2] S. Coleman, *Aspects of symmetry: selected Erice lectures* (Cambridge University Press, 1988).
[3] N. S. Manton and P. Sutcliffe, *Topological solitons* (Cambridge University Press, 2004).
[4] A. Vilenkin and E. P. S. Shellard, *Cosmic Strings and Other Topological Defects* (Cambridge University Press, 2000).
[5] G. E. Volovik, *The universe in a helium droplet*, Vol. 117 (Oxford University Press on Demand, 2003).
[6] D. R. Nelson, *Defects and Geometry in Condensed Matter Physics 1st Edition* (Cambridge University Press, 2002) p. 392.
[7] A. N. Bogdanov and D. Yablonskii, Zh. Eksp. Teor. Fiz **95**, 178 (1989).
[8] A. Bogdanov and A. Hubert, Journal of Magnetism and Magnetic Materials **138**, 255 (1994).
[9] U. Rößler, A. Bogdanov, and C. Pfleiderer, Nature **442**, 797 (2006).
[10] B. Binz, A. Vishwanath, and V. Aji, Phys. Rev. Lett. **96**, 207202 (2006).
[11] I. Dzyaloshinsky, Journal of Physics and Chemistry of Solids **4**, 241 (1958).
[12] T. Moriya, Phys. Rev. **120**, 91 (1960).
[13] Y. Togawa, T. Koyama, K. Takayanagi, S. Mori, Y. Kousaka, J. Akimitsu, S. Nishihara, K. Inoue, A. S. Ovchinnikov, and J. Kishine, Phys. Rev. Lett. **108**, 107202 (2012).
[14] J.-i. Kishine and A. Ovchinnikov, in *Solid State Physics*, Vol. 66 (Elsevier, 2015) pp. 1–130.
[15] Y. Togawa, Y. Kousaka, K. Inoue, and J.-i. Kishine, Journal of the Physical Society of Japan **85**, 112001 (2016).
[16] S. Mühlbauer, B. Binz, F. Jonietz, C. Pfleiderer, A. Rosch, A. Neubauer, R. Georgii, and P. Böni, Science **323**, 915 (2009).
[17] X. Yu, Y. Onose, N. Kanazawa, J. Park, J. Han, Y. Matsui, N. Nagaosa, and Y. Tokura, Nature **465**, 901 (2010).
[18] S. Heinze, K. Von Bergmann, M. Menzel, J. Brede, A. Kubetzka, R. Wiesendanger, G. Bihlmayer, and S. Blügel, Nature Physics **7**, 713 (2011).
[19] N. Nagaosa and Y. Tokura, Nature nanotechnology **8**, 899 (2013).
[20] J. H. Han, J. Zang, Z. Yang, J.-H. Park, and N. Nagaosa, Phys. Rev. B **82**, 094429 (2010).
[21] M. Ezawa, Phys. Rev. **B83**, 100408 (2011).
[22] A. Goussev, J. M. Robbins, V. Slastikov, and O. A. Tretiakov, Phys. Rev. B **93**, 054418 (2016).
[23] V. E. Timofeev, A. O. Sorokin, and D. N. Aristov, JETP Letters **109**, 207 (2019).
[24] P. Milde, D. Köhler, J. Seidel, L. M. Eng, A. Bauer, A. Chacon, J. Kindervater, S. Mühlbauer, C. Pfleiderer, S. Buhrandt, C. Schütte, and A. Rosch, Science **340**, 1076 (2013).
[25] N. Kanazawa, Y. Nii, X. X. Zhang, A. S. Mishchenko, G. De Filippis, F. Kagawa, Y. Iwasa, N. Nagaosa, and Y. Tokura, Nature Communications **7**, 11622 (2016).
[26] A. Zheludev, S. Maslov, G. Shirane, Y. Sasago, N. Koide, and K. Uchinokura, Phys. Rev. Lett. **78**, 4857 (1997).
[27] J. Chovan, N. Papanicolaou, and S. Komineas, Phys. Rev. B **65**, 064433 (2002).
[28] A. N. Bogdanov, U. K. Rößler, M. Wolf, and K.-H. Müller, Phys. Rev. B **66**, 214410 (2002).
[29] G. Gitgeatpong, Y. Zhao, P. Piyawongwatthana, Y. Qiu, L. W. Harriger, N. P. Butch, T. J. Sato, and K. Matan, Phys. Rev. Lett. **119**, 047201 (2017).
[30] S. Mühlbauer, G. Brandl, M. Månsson, and M. Garst, Phys. Rev. B **96**, 134409 (2017).
[31] B. Barton-Singer, C. Ross, and B. J. Schroers, Commun. Math. Phys. (2020), 10.1007/s00220-019-03676-1.
[32] C. Adam, J. M. Queiruga, and A. Wereszczynski, JHEP **07**, 164 (2019).
[33] C. Adam, K. Oles, T. Romanczukiewicz, and A. Wereszczynski, (2019), arXiv:1902.07227 [cond-mat.mes-hall].
[34] B. J. Schroers, SciPost Phys. **7**, 030 (2019).
[35] E. B. Bogomolny, Sov. J. Nucl. Phys. (1976).
[36] M. K. Prasad and C. M. Sommerfield, Phys. Rev. Lett. **35**, 760 (1975).
[37] A. A. Belavin, A. M. Polyakov, A. S. Schwartz, and Yu. S. Tyupkin, Phys. Lett. **B59**, 85 (1975).
[38] A. M. Polyakov and A. A. Belavin, JETP Lett. **22**, 245 (1975).
[39] G. 't Hooft, Phys. Rev. **D14**, 3432 (1976).
[40] G. 't Hooft, Phys. Rev. Lett. **37**, 8 (1976).
[41] R. Jackiw and C. Rebbi, Phys. Rev. Lett. **37**, 172 (1976).
[42] C. G. Callan, Jr., R. F. Dashen, and D. J. Gross, Phys. Lett. **B63**, 334 (1976).
[43] T. Schäfer and E. V. Shuryak, Rev. Mod. Phys. **70**, 323 (1998).
[44] T. A. Kaplan, Zeitschrift für Physik B Condensed Matter **49**, 313 (1983).
[45] L. Shekhtman, O. Entin-Wohlman, and A. Aharony, Phys. Rev. Lett. **69**, 836 (1992).
[46] E. Galkina and B. Ivanov, Low Temperature Physics **44**, 618 (2018).
[47] The equivalence theorem discussed later will show that this seemingly *ad hoc* way to find the ground state is true in our one-dimensional model.
[48] Effective theory of ferromagnetic material involves the first order term in time derivative, instead of the second order.
[49] T. Fujimori, S. Kamata, T. Misumi, M. Nitta, and N. Sakai, Phys. Rev. **D94**, 105002 (2016).
[50] T. Fujimori, S. Kamata, T. Misumi, M. Nitta, and N. Sakai, Phys. Rev. **D95**, 105001 (2017).
[51] G. V. Dunne and M. Unsal, Phys. Rev. **D87**, 025015 (2013).
[52] G. V. Dunne and M. Unsal, Ann. Rev. Nucl. Part. Sci. **66**, 245 (2016).
[53] T. Misumi, M. Nitta, and N. Sakai, JHEP **06**, 164 (2014).
[54] T. Misumi, M. Nitta, and N. Sakai, PTEP **2015**, 033B02 (2015).
[55] T. Misumi, M. Nitta, and N. Sakai, JHEP **09**, 157 (2015).
[56] T. Fujimori, S. Kamata, T. Misumi, M. Nitta, and N. Sakai, PTEP **2017**, 083B02 (2017).

[57] T. Fujimori, S. Kamata, T. Misumi, M. Nitta, and N. Sakai, JHEP **02**, 190 (2019).
[58] M. Nitta and W. Vinci, J. Phys. **A45**, 175401 (2012).
[59] J. Jaykka and M. Speight, Phys. Rev. **D82**, 125030 (2010).
[60] M. Kobayashi and M. Nitta, Phys. Rev. **D87**, 125013 (2013).
[61] M. Eto, Y. Isozumi, M. Nitta, K. Ohashi, and N. Sakai, Phys. Rev. **D72**, 025011 (2005).
[62] M. Eto, T. Fujimori, Y. Isozumi, M. Nitta, K. Ohashi, K. Ohta, and N. Sakai, Phys. Rev. **D73**, 085008 (2006).
[63] M. Eto, Y. Isozumi, M. Nitta, K. Ohashi, and N. Sakai, J. Phys. **A39**, R315 (2006).
[64] When our system is put in the finite interval $0 \leq x \leq L$, we also need to take account of the change of the boundary condition.
[65] K. Ohashi, T. Fujimori, and M. Nitta, Phys. Rev. **A96**, 051601(R) (2017).
[66] D. A. Takahashi, K. Ohashi, T. Fujimori, and M. Nitta, Phys. Rev. **A96**, 023626 (2017).
[67] S.-A. Siegfried, E. V. Altynbaev, N. M. Chubova, V. Dyadkin, D. Chernyshov, E. V. Moskvin, D. Menzel, A. Heinemann, A. Schreyer, and S. V. Grigoriev, Phys. Rev. B **91**, 184406 (2015).
[68] T. Koretsune, N. Nagaosa, and R. Arita, Scientific Reports **5**, 13302 (2015).
[69] A. Belabbes, G. Bihlmayer, S. Blügel, and A. Manchon, Scientific Reports **6**, 24634 (2016).
[70] X. Ma, G. Yu, X. Li, T. Wang, D. Wu, K. S. Olsson, Z. Chu, K. An, J. Q. Xiao, K. L. Wang, and X. Li, Phys. Rev. B **94**, 180408(R) (2016).
[71] F. D. M. Haldane, Phys. Rev. Lett. **50**, 1153 (1983).
[72] F. D. M. Haldane, Phys. Lett. **A93**, 464 (1983).
[73] F. D. M. Haldane, Phys. Rev. Lett. **61**, 1029 (1988).
[74] N. Read and S. Sachdev, Phys. Rev. Lett. **62**, 1694 (1989).
[75] T. Senthil, A. Vishwanath, L. Balents, S. Sachdev, and M. P. A. Fisher, Science **303**, 1490 (2004).
[76] E. H. Lieb, T. Schultz, and D. Mattis, Annals Phys. **16**, 407 (1961).
[77] I. Affleck and E. H. Lieb, Lett. Math. Phys. **12**, 57 (1986).
[78] N. Nagaosa, *Quantum field theory in strongly correlated electronic systems* (Springer Science & Business Media, 1999).
[79] E. Fradkin, *Field Theories of Condensed Matter Physics* (Cambridge University Press, 2013) p. 856.
[80] E. C. Marino, *Quantum field theory approach to condensed matter physics* (Cambridge University Press, 2017).